EJN fens EUROPEAN JOURNAL OF NEUROSCIENCE

European Journal of Neuroscience, pp. 1–14, 2013 doi:10.1111/ejn.12267

Modulation of presynaptic Ca^{2+} currents in frog motor nerve terminals by high pressure

Ben Aviner,[1,*] Gideon Gradwohl,[2,*] Homer J. Moore[3] and Yoram Grossman[1]
[1]Department of Physiology and Neurobiology, Faculty of Health Science and Zlotowski Center for Neuroscience, Ben-Gurion University of the Negev, Beer-Sheva, 84105, Israel
[2]Department of Physics, Jerusalem College of Technology, Jerusalem, Israel
[3]Department of Neurology, University of Florida, College of Medicine, Gainesville, FL, USA

Keywords: hyperbaric pressure, nerve terminal, neuromuscular junction, synaptic transmission

Abstract

Presynaptic Ca^{2+}-dependent mechanisms have already been implicated in depression of evoked synaptic transmission by high pressure (HP). Therefore, pressure effects on terminal Ca^{2+} currents were studied in *Rana pipiens* peripheral motor nerves. The terminal currents, evoked by nerve or direct stimulation, were recorded under the nerve perineurial sheath with a loose macropatch clamp technique. The combined use of Na^+ and K^+ channel blockers, $[Ca^{2+}]_o$ changes, voltage-dependent Ca^{2+} channel (VDCC) blocker treatments and HP perturbations revealed two components of presynaptic Ca^{2+} currents: an early fast Ca^{2+} current (I_{CaF}), possibly carried by N-type ($Ca_V2.2$) Ca^{2+} channels, and a late slow Ca^{2+} current (I_{CaS}), possibly mediated by L-type (Ca_V1) Ca^{2+} channels. HP reduced the amplitude and decreased the maximum (saturation level) of the Ca^{2+} currents, I_{CaF} being more sensitive to pressure, and may have slightly shifted the voltage dependence. HP also moderately diminished the Na^+ action current, which contributed to the depression of VDCC currents. Computer-based modeling was used to verify the interpretation of the currents and investigate the influence of HP on the presynaptic currents. The direct HP reduction of the VDCC currents and the indirect effect of the action potential decrease are probably the major cause of pressure depression of synaptic release.

Introduction

Exposure to high pressure (HP) (> 1.0 MPa) profoundly depresses evoked excitatory transmission in a variety of vertebrate (Kendig *et al.*, 1975; Kendig & Cohen, 1976) and invertebrate (Campenot, 1975; Henderson *et al.*, 1977; Parmentier *et al.*, 1981; Grossman & Kendig, 1988) synapses. The uniformity of the response in all chemical synapses, excitatory as well as inhibitory (Colton & Colton, 1982; Grossman & Kendig, 1988), suggests that the pressure primarily diminishes a presynaptic process, i.e. transmitter release from the presynaptic terminals (Campenot, 1975; Ashford *et al.*, 1982; Grossman *et al.*, 1991a) or synaptosomes (Gilman *et al.*, 1986a, 1989), rather than affecting the maximal currents in different postsynaptic receptors (Parmentier *et al.*, 1981; Heinemann *et al.*, 1987; Shelton *et al.*, 1990; Macdonald *et al.*, 1993). However, pressure may also decrease neurotransmission by interfering with the function of specific neurotransmitter receptors (Shelton *et al.*, 1993; Mor *et al.*, 2008). Pressure could impede the inflow of Ca^{2+} into the nerve terminals, which is an important step in the release process [for review, see Aviner *et al.*, 2010)]. Early measurements of HP depression of voltage-dependent radiolabeled Ca^{2+} uptake into brain synaptosomes (Gilman *et al.*, 1986b) suggested this possibility. The relationship between external Ca^{2+} and single and facilitated invertebrate synaptic potentials (Grossman & Kendig, 1990) or synaptic currents (Grossman *et al.*, 1991a; Golan & Grossman, 1992) at HP, and similar responses of field potentials in rat cerebellar and hippocampal brain slices (Etzion & Grossman, 1999, 2000; Talpalar *et al.*, 2010), indirectly support the hypothesis that pressure reduces the maximal voltage-dependent Ca^{2+} channel (VDCC)-mediated Ca^{2+} influx into the presynaptic terminal.

Preliminary results (Aviner *et al.*, 2009) suggest that pressure may selectively affect Ca^{2+} currents in specific VDCCs expressed in frog oocytes. However, more direct evidence is necessary in order to establish this notion in axonal presynaptic terminals.

Voltage-dependent Ca^{2+} channels are members of a superfamily of transmembrane ion channel proteins that includes voltage-gated K^+ and Na^+ channels (Yu & Catterall, 2004). Various VDCC types exist, composed of four or five distinct subunits (α_1, α_2, δ, β, γ) that are encoded by multiple genes (Catterall, 2000). Traditionally, the different Ca^{2+} currents were defined by physiological and pharmacological properties (Tsien *et al.*, 1988; Bean, 1989; Hess, 1990), and were termed L, P/Q, N, R and T types, but a modern nomenclature is also in use: the Ca_V1, Ca_V2 and Ca_V3 families, respectively. In addition to its role in synaptic release, the transient Ca^{2+} influx (leading to a cytosolic $[Ca^{2+}]$ increase) controls neuronal excitability,

Correspondence: Dr Ben Aviner, as above.
E-mail: aviner@post.bgu.ac.il

*B.A. and G.G. contributed equally to this work.

Received 27 June 2012, revised 17 April 2013, accepted 29 April 2013

© 2013 Federation of European Neuroscience Societies and John Wiley & Sons Ltd

initiates excitation–contraction coupling, hormone secretion, and ciliary movement, and activates various signaling pathways, including gene expression.

The methodology of recording voltage signals extracellularly under the perineurial sheath proximal to the motor nerve terminals of the frog (Gundersen *et al.*, 1982; Mallart, 1984; Hevron *et al.*, 1986; Anderson *et al.*, 1988), the mouse (Brigant & Mallart, 1982; Mallart, 1985; Penner & Dreyer, 1986), the lizard (Lindgren & Moore, 1989, 1991) and the chick (Stanley, 1989) has been used successfully to study the ionic currents in the motor nerve terminals. Using a similar, although modified, loose patch clamp technique, we examined the effect of HP on Na^+ and Ca^{2+} currents in frog nerve terminals. The data demonstrate a considerable, although differential, pressure-dependent reduction in fast inactivating (N-type-like) and slow inactivating (L-type-like) Ca^{2+} currents, associated with a moderate decrease in the Na^+ action current.

A computer simulation model was used to verify the analysis of the experimental perineurial current recorded at the node of Ranvier. We successfully reconstructed this extracellular current by synthesis of individual ionic currents [Na^+ current (I_{Na}), I_{Ca}, and K^+ current (I_K)] at both the node and the axonal terminal (end plate). By adjusting the magnitude and the kinetics of I_{Na}, I_{Ca} and I_K blockade under various conditions, we were also able to simulate the pressure effects.

The combination of simulation and experimental data strongly indicate that the reduction in the terminal VDCC current is caused directly by HP, and also indirectly by the moderate reduction in I_{Na} caused by the same pressure. This indicates that I_{Ca} reduction is one of the major factors determining the depression of synaptic release (i.e. transmission) under hyperbaric pressure conditions.

Materials and methods

Preparation and solutions

Frogs (*Rana pipiens*) were obtained from a local dealer, and kept in fresh-water containers in an air-conditioned room at a temperature of 18–19 °C. Experiments were carried out during early spring or autumn. Cutaneous pectoris nerve–muscle preparations were dissected from the frog as previously described (Braun & Schmidt, 1966; Mallart, 1984). The muscle was mounted in an experimental bath constantly perfused with physiological solution aerated at ambient pressure. The normal perfusate had the following composition : 116 mM NaCl; 2 mM KCl; 1.8 mM $CaCl_2$; 5 mM Tris buffer; pH 7.4. The temperature was monitored with a thermistor next to the preparation, and was maintained at 18 °C. d-Tubocurarine (5 mg/L), a nicotinic acetylcholine receptor inhibitor, was added to block synaptic transmission and muscle contraction. Excess of thin connective tissue, which covers the muscle surface, was manually removed. The bath was placed in a hyperbaric chamber equipped for remote-controlled neurophysiological studies (Grossman *et al.*, 1991a). Drugs, toxins and divalent ions, which were used in low concentrations to block various channels, were added to the physiological solution. Tetraethyl ammonium (TEA) was applied (10 mM) throughout all experiments in order to block all types of I_K current and reveal the Ca^{2+} current (see below). The L-type VDCC blocker nifedipine was first dissolved in ethanol, and then diluted to the desired concentration in the perfusate. Experiments with this drug were carried out in very dim light, owing to its photosensitivity. The solutions were introduced to the chamber with an HP pump (Milton-Roy, USA). The rate of perfusion was 6–8 mL/min, which was equal to a change of three to four bath volumes per minute. This experimental procedure and animal use were approved by the Naval Medical Research Institute and Ben Gurion University of the Negev ethics committees.

Stimulation and recording

After the chamber had been sealed, the perineurial sheath of a superficial preterminal nerve bundle was impaled with an NaCl-filled (1 M) microelectrode (2–5 MΩ). This was accomplished by using a *Z*-axis microstepper (Transvertex, Sweden) and *X*–*Y* microtranslators (Oriel, USA). The whole procedure was monitored with a video camera mounted on a 4-inch reflecting microscope (Questar, USA) positioned outside the chamber in front of a Plexiglas view port (Grossman *et al.*, 1991a). The potential below the electrode tip was clamped to ground (zero) potential (Dagan model 8800; Dagan, USA), with a loose patch clamp technique (Parnas *et al.*, 1982). Under these conditions, it was possible to extracellularly record the circuit currents flowing between the terminals and the parent axons (Fig. 1, node 2) following stimulation of the main nerve by a distally located suction electrode (Fig. 1, node *n*). Examples of the control current are shown in Figs 2A (control) and Fig. 3B (control). The current records showed low noise and were relatively stable. During the experiment, the nerve was stimulated at 0.2 Hz in order to verify the viability and stability of the preparation. Averaging of the responses during the desired time periods was performed off-line.

As the present study is the first to employ perineurial current measurement at pressure, we tested for possible mechanical artefacts resulting from pressure application. In preliminary experiments at normal pressure, the electrode was withdrawn from its optimal position with 1–2-μm steps of the micromanipulator. For each step, the normalised (percentage of control) peak K^+ current was plotted as a function of the normalised peak of the concomitant Na^+ current (not shown). The electrode was then inserted back into its original position, and TEA was added in order to block all K^+ currents, revealing

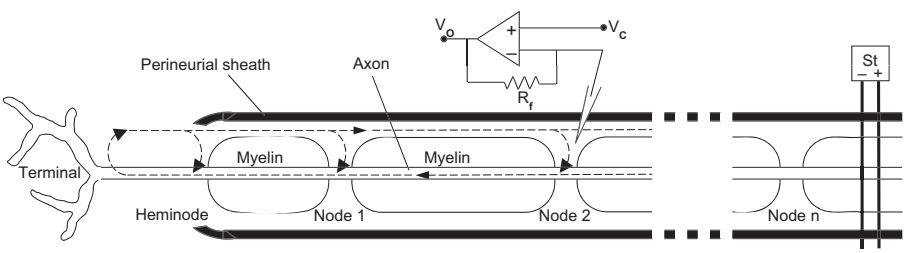

FIG. 1. Simplified diagram of the terminal part of the frog motor nerve. Dashed thin lines indicate current pathways, and arrows indicate their direction of flow. The point of electrode penetration was most probably not next to the very first node, but next to an adjacent one, e.g. node 2. Modified from Mallart (1985). R_f, feedback resistance; St, stimulus; V_c, command voltage; V_o, output voltage.

© 2013 Federation of European Neuroscience Societies and John Wiley & Sons Ltd

the Ca^{2+} current components (Fig. 2). The same procedure of electrode withdrawal and peak amplitude normalisation was repeated for the fast Ca^{2+} current and Na^{+} currents.

We found that both K^{+} and Ca^{2+} currents and the Na^{+} current were similarly reduced by withdrawing the recording electrode, despite their different sites of origin, indicating that the actual differential effect of HP is not a mechanical artefact (data not shown).

Direct stimulation

Direct stimulation of the terminals and recording of the resulting currents (Fig. 1, node 2) (Parnas *et al.*, 1982) were achieved by use of a macropatch clamp amplifier specifically designed to accommodate patch electrodes with a resistance of up to 10 MΩ (Zeitz Instruments Model 8510; Zeitz Instruments, Germany). The circuit specifications, the use of the patch electrodes and the benefits of the method are described and discussed in detail in Parnas *et al.* (1982). Briefly, the positive or negative pulses saturate the input stage, which recovers very rapidly; however, unavoidable capacitive artefacts following the pulse had to be compensated for beyond the input stage by subtraction of a complementary artefact waveform generated by a special circuit. Negative pulses (0.1–1.0 μA; duration, 1–3 ms) depolarised the axon membranes and evoked responses, whereas the corresponding positive pulses were ineffective. Because, under the perineurial sheath in the vicinity of the axons, the large current response of the terminals immediately followed the end of the stimulating negative pulse, it was impossible to compensate for its concomitant artefact. Therefore, for any chosen intensity, the artefact was optimally compensated for only the positive polarity, and the terminals were then stimulated 10 times at 0.5 Hz with an otherwise identical negative pulse, and averaged online. In an off-line analysis, the compensated current trace evoked by the positive pulse was digitally subtracted from its corresponding negative stimulus record to reveal the net terminal response.

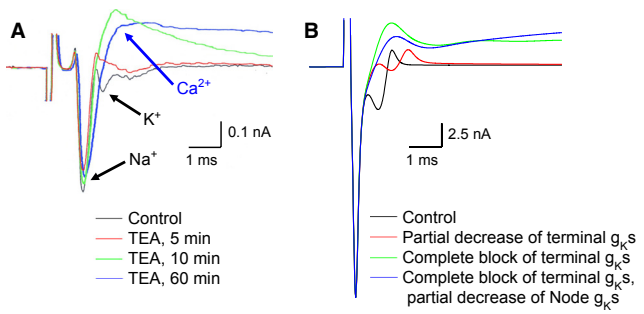

FIG. 2. (A) TEA (10 mM) blocks K^{+} currents and reveals the Ca^{2+} current component. The time of drug application is indicated. (B) Progressive decrease of g_K in the computer simulation.

Experimental protocol

After establishment of a stable recording, the preparation was perfused with physiological solution containing TEA during all experiments (as above). Perfusion for 20–30 min was sufficient to stabilise the resultant recordings. Control measurements of the unmasked Ca^{2+} currents were made after 40 min, and this was followed by helium compression to pressures of 1.8, 2.3, 3.5, 4.6, 5.2 and 6.9 MPa (usually not all steps for each experiment, owing to viability concerns) at a compression rate of 0.2 MPa/min. Recordings at each pressure step were made after a minimum of 20 min, to allow the temperature to return to the control level after the transient increase (1–3 °C) and the preparation to stabilise (Grossman &

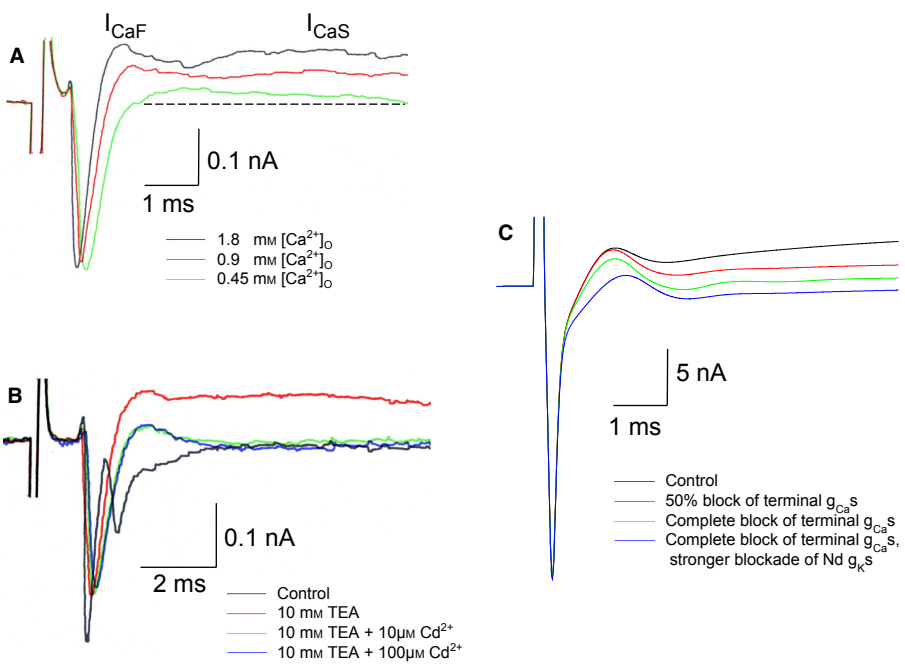

FIG. 3. (A) $[Ca^{2+}]_o$ dependence of the fast (I_{CaF}) and slow (I_{CaS}) Ca^{2+} currents at the terminal. The dashed line indicates baseline (zero) current. Both currents are diminished by reduced $[Ca^{2+}]_o$. All traces were recorded after TEA application. (B) Cd^{2+} blocks Ca^{2+} currents. Cd^{2+} at 10 μM blocks both fast and slow Ca^{2+} currents. Increasing the concentration to 100 μM does not enhance the effect. The remaining positive phase probably reflects conducted AP beyond the point of recording (back reflection), and not a residual Ca^{2+} current (see Fig. 7). (C) Reduction of Ca^{2+} (g_{Ca}) in the computer simulation, imitating reduced extracellular Ca^{2+} or VDCC blockade. In 'Control' – conductance parameters are equal to those in Fig. 2B, blue. Nd, nodal.

© 2013 Federation of European Neuroscience Societies and John Wiley & Sons Ltd

Kendig, 1984, 1986). Decompression to 0.1–0.3 MPa was always attempted, but was successful in only 35% of the experiments.

Analysis

Currents were amplified (bandpass DC 3 kHz for the Dagan amplifier, and DC 9 kHz for the Zeitz amplifier), viewed on a digital oscilloscope, digitised (Labmaster; Scientific Solutions, USA), and stored for later analysis with computer-based software (PCLAMP; Axon Instruments, USA). Where appropriate, results were analysed for statistical significance with Student's paired *t*-test, with each preparation as its own control.

Computer simulations

The electric currents beneath the perineurial sheath wrapping the frog nerve fibers were simulated with a computer model representing the axon terminal, the nodes of Ranvier, and the intersegmental compartments (Fig. 1), based on morphological and electrophysiological experiments in mouse and frog terminals (Mallart, 1984, 1985). The simulation model was executed by the NEURON simulator (Hines, 1989). Na^+, K^+ and Ca^{2+} channels were inserted at specific locations, imitating their postulated axonal distribution. The total current was evaluated at the node located most proximally to the axon terminal (Fig. 1, node 1). The extracellular current at the recording site was produced by local currents, currents between the myelinated axon and the perineurial sheath, and currents initiated at the terminal and reflected passively to node 1. We used the right portion of Eqn 1 to calculate the total membrane current:

$$I_{\text{total}} = C_{\text{m}}\frac{\mathrm{d}v_j}{\mathrm{d}t} + i_{\text{ion}} = \frac{D}{4R_{\text{a}}}\cdot\frac{v_{j+1} - 2v_j + v_{j-1}}{\Delta x^2} \qquad (1)$$

where index j describes the segment of the recording site and $j - 1$ and $j + 1$ are the neighboring segments, Δx is the length of the segment j, and D is its diameter, R_{a} is the axial specific resistance of the axon, C_{m} is the capacity, v is the membrane potential, and i_{ion} is the sum of the different ionic currents. The model included five nodes of Ranvier, each of diameter 5 μm diameter and length 1.8 μm, and a heminode with the same diameter but a length of 1 μm. The axon terminal diameter and length were 5 and 25 μm, respectively. The estimated 'unusual' length of the terminal reflects the branching at the end plate. A short 'extra' segment was added at the terminal end with very high intracellular and membrane resistances in order to simulate a sealed end of the terminal. The internode length was 70 μm, and it was 25 μm from to the heminode. The capacities at the different segments were: 1 μF/cm^2 at the terminal, 2 μF/cm^2 at the nodes/heminode, and 0.1 μF/cm^2 at the internodes. The intracellular resistance was 1000 Ω/cm at the sealed end segment, and 70 Ω/cm at the other compartments. The resting potential was set to −70 mV. Channels characteristic of Na^+, delayed rectifier K^+ (K_{DR}), slow K^+ (K_S) (Traub & Miles, 1991), L-type Ca^{2+} and N-type Ca^{2+} (Booth *et al.*, 1997) were inserted at the axon terminal. Similar Na^+, K_{DR} and K_S channels with relatively higher conductance density (g) were inserted in the nodes, but with no g_{Ca}. The other internode compartments remained passive. The stimulation step current was injected either at node 5 to simulate nerve stimulation, or at node 1, the model recording site, to simulate the 'direct stimulation' method experiments (see above). The model is obviously simplified, lacking possible additional voltage-dependent channels and other active compartments. However, it was intended to facilitate the analysis under hyperbaric conditions of the terminal–node 1 interactions as reflected by the extracellular currents.

Results

TEA-disclosed Ca^{2+} currents

The characteristic currents flowing at the recording site under the perineurial sheath are shown in Fig. 2(A) (control) and Fig. 3(B) (control). The early short positive (upward) phase (after the stimulus artefact) represents the passive depolarisation of the axons by propagating the action potential (AP). The first negative (downward) component represents the large AP Na^+ inward current at the nodes, which leads to terminal depolarisation. The second smaller negative component reflects the outward K^+ current at the remote repolarising terminals, and possibly from node 1 (Mallart, 1984, 1985; Hevron *et al.*, 1986), and thus measured at the node as an inward current. The interruption between the two negative peaks may represent a short local outward K^+ current as part of the nodal AP (see modeling below). Application of TEA, a K^+ channel blocker (10 mM, non-specific concentration) (Stanfield, 1983), abolished the second current negativity in a time-dependent manner (Fig. 2A; TEA 5 min), slightly widened the first negative component, and disclosed a large outward current (Fig. 2A; TEA 10 min), which stabilised after 20–30 min as a long-duration outward current that could be recorded for several hours (Fig. 2A; TEA 60 min). This current was $[Ca^{2+}]_o$-dependent; an example of the decreased current during exposure to reduced $[Ca^{2+}]_o$ is shown in Fig. 3A. This Ca^{2+} current was composed of two overlapping phases: a fast transient phase that followed the end of the Na^+ current (I_{CaF}), and a slow phase (I_{CaS}) (Fig. 3A and B). I_{CaF} reached its peak within 1–4 ms, whereas I_{CaS} usually reached its peak within 8–12 ms, similar to the known activation times for VDCCs (Byerly *et al.*, 1984; Boland & Bean, 1993; Formenti *et al.*, 1998; Artim & Meriney, 2000; O'Connell & Dirksen, 2000). These two separate peaks, or their corresponding time windows (when absolute peaks were not clear), were used for measurement of the amplitudes of I_{CaF} and I_{CaS}.

To further verify the role of Ca^{2+} in this current, we tested the effect of Cd^{2+} blockade. Application of 10 μM Cd^{2+} blocked both I_{CaF} and I_{CaS} (Fig. 3B). At this concentration, Cd^{2+} is known to block various types of VDCC, including N-type and L-type VDCCs. The remaining small positive deflection, which was not blocked even by 100 μM Cd^{2+} (Fig. 3B), is most probably a passive back reflection of the AP from a distal terminal site (Grossman *et al.*, 1979) carried by K^+ ions at the node via residual g_K in the presence of TEA (see Simulation below and Discussion). Therefore, these two phases of the positive deflection were identified as inward Ca^{2+} flux at the terminal.

Simulation of TEA blockade of I_K and I_{Ca} modification

The following values of the ionic conductances were found to best simulate (Fig. 2B, control) the experimental control nodal currents (Fig. 2A, control) at atmospheric pressure (in S/cm^2): at the terminal, Na^+ (g_{Na}) = 0.11, delayed rectifier K^+ (g_{KDR}) = 0.42, slow K^+ conductance density (g_{Ks}) = 0.05, N-type Ca^{2+} (g_{CaN}) = 0.01, and L-type Ca^{2+} (g_{CaL}) = 0.0025; and at the node, g_{Na} = 1.6, g_{KDR} = 0.26, and g_{Ks} = 1.0 (Fig. 2B, black line).

In order to verify our interpretation of the TEA effects, the time-dependent blockade of the two I_Ks (Fig. 2A) was simulated by decreasing g_K in gradual steps, as detailed in Table 1.

© 2013 Federation of European Neuroscience Societies and John Wiley & Sons Ltd

TABLE 1. Channel blockade in simulation of TEA effect

Step	Terminal (% block) g_{KDR}	Terminal (% block) g_{Ks}	Node (% block) g_{KDR}	Fig. 2(A)
a	80	80	–	TEA 5 min, red trace
b	100	100	–	TEA 10 min, green trace
c	100	100	60	TEA 60 min, blue trace

TABLE 2. Channel blockade in simulation of $[Ca^{2+}]_o$ reduction and Cd^{2+} blockade effects

Step	Terminal (% block) g_{KDR}	Terminal (% block) g_{Ks}	Terminal (% block) $g_{Ca(F\&S)}$	Node (% block) g_{KDR}	Node (% block) g_{Ks}	Fig. 3(C)
a	100	100	50	60	–	Red line
b	100	100	100	80	–	Green line
c	100	100	100	92	50	Blue line

Interestingly, the outward current in step b is larger than in step c (also observed experimentally), as the nodal I_K is not blocked. In step c, the long-duration I_{CaS} could be detected. It was impossible to cancel the total g_Ks at all the segments of the model, because the remaining g_{Ca} caused oscillations, a phenomenon that was not observed in the experiments. This set of simulations fits quite well with the experimental data, and suggests a time-dependent gradual blockade of various I_Ks from the exposed terminal to the concealed node. Furthermore, it suggests that, under the steady-state conditions for measuring I_{Ca}, some residual I_K is present at the nodes.

$[Ca^{2+}]_o$ reduction (Fig 3A) and Cd^{2+} blockade (Fig. 3B) were used to demonstrate that the fast and slow phases of the disclosed current are indeed Ca^{2+} currents. We simulated these conditions (Fig. 3C) by equally decreasing both types of g_{Ca}, as detailed in Table 2.

The simulation successfully replicated the experimental results, supporting the notion that the long-duration positive deflection represents fast and slow components of Ca^{2+} current. However, it also indicated that the early positive 'hump' of the current, in addition to being a passive back reflection of the AP from the terminal (as suggested by the experimental results), could also represent a partially active I_K, as residual g_Ks probably remain at the node, a fact that would prevent voltage oscillation.

Characterisation of the Ca^{2+} currents

After establishment of the nature of the long-duration current as a terminal Ca^{2+} current, various VDCC blockers were applied in order to identify the types of channel associated with it (see Table 6).

Ni^{2+}

The effect of Ni^{2+}, which is known to block T-type VDCCs at 10 μM, and N-type and L-type channels at > 100 μM, was examined (Fig. 4A). A dose–response curve (Fig. 4C) revealed that 15 μM had no significant effect on the currents, excluding the involvement of T-type VDCCs. Ni^{2+} at 25–50 μM reduced the amplitude of I_{CaF} by 65%, concomitantly with an only 18–22% decrease in I_{CaS}. This differential effect was highly significant (Fig. 4C, arrows). The I_{Na} amplitude was not significantly affected.

Cd^{2+}

Cd^{2+} (10 μM) blocked both I_{CaF} and I_{CaS} (Fig. 3B, green trace). At this concentration, Cd^{2+} is known to block N-type and L-type VDCCs (n = 4). Therefore, it was used to block all Ca^{2+} currents at the terminal.

Phenytoin

This antiepileptic drug has been implicated in blocking T-type channels at concentrations as low as 1 μM (Hevron *et al.*, 1986; Yaari *et al.*, 1987). Under such conditions, the drug had no effect on any of the Ca^{2+} currents. Phenytoin similarly suppressed both Ca^{2+} currents only at much higher (probably non-specific) concentrations (ED_{50} = 50 μM, n = 3). This indicates again the lack of T-type VDCC involvement in the frog terminal currents.

Nifedipine (dihydropiridine)

The effect of nifedipine, a well-known L-type VDCC blocker, was examined (Fig. 4B). A dose–response curve of nifedipine (Fig. 4D) revealed that 25 μM reduced I_{CaS} by 90%, whereas I_{CaF} was reduced by 32%. This differential effect was highly significant (Fig. 4D, arrows). A concentration of 30 μM had a slightly lesser effect, although it was differential and significant. A concentration of 50 μM completely blocked both currents (Fig. 4B).

Bay K 8644

As expected, the L-type channel agonist had no effect on I_{CaF} at concentrations up to 10 μM. The drug slightly increased (10%) I_{CaS} (n = 3).

Despite some inconsistencies of the responses relative to what is generally known of the effects of the drugs, the combined data suggest that I_{CaF} is carried by N-type VDCCs and that I_{CaS} is mediated by one of the L-type VDCCs. Ni^{2+} (as an 'I_{CaF} blocker') and nifedipine (as an 'I_{CaS} blocker') were used in subsequent experiments as a means for studying pressure effects on each current separately.

Pressure effects on Ca^{2+} currents

High pressure depressed Ca^{2+} currents in a pressure-dependent manner (Fig. 5C). At 6.9 MPa, the peak amplitude of the maximal Ca^{2+} current was suppressed by 85 ± 5% (mean ± standard error of the mean, n = 6). Concomitantly, the Na^+ action current was reduced by 25 ± 10%. A significant reduction of 40 ± 4% (n = 11) in the Ca^{2+} current was also observed at much lower pressure of 1.8 MPa.

In the above series of experiments, no attempt was made to separate the specific Ca^{2+} currents. In order to clearly reveal pressure effects on each current phase, compression was carried out in the presence of either 25 μM Ni^{2+} (partially blocking I_{CaF}; Fig. 5A), representing mostly I_{CaS}, or 25 μM nifedipine (which reduced I_{CaS}; Fig. 5B), representing mostly I_{CaF}. Pressure depressed I_{CaS} almost linearly. I_{CaF} was more sensitive to the lower pressure range, showing approximately 42 ± 7% (n = 7) depression at 1.8 MPa, as compared with an estimated (interpolation) 21% reduction of I_{CaS} at the same pressure (Fig. 5D). The I_{CaF} experiments were carried out at four pressure steps (instead of three for I_{CaS}), starting at a lower pressure, as we suspected that this current had higher pressure sensitivity (Etzion & Grossman, 2000).

© 2013 Federation of European Neuroscience Societies and John Wiley & Sons Ltd

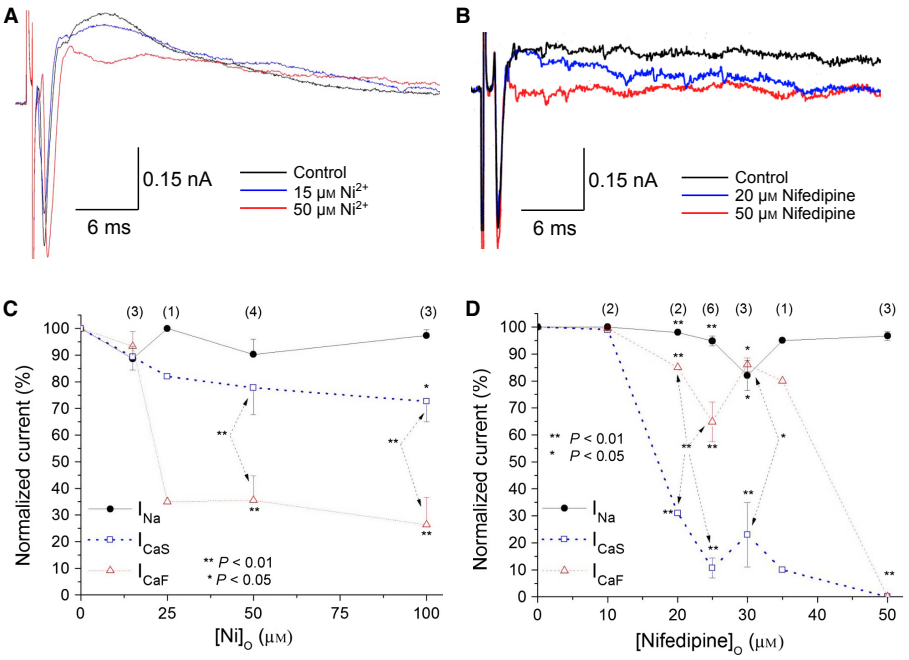

FIG. 4. Selective effects of Ni^{2+} and nifedipine on the Ca^{2+} currents. Bars indicate standard errors of the mean; numbers in parentheses indicate *n*. (A) Traces recorded in the presence of increasing concentrations of Ni^{2+}. (B) Traces recorded in the presence of increasing concentrations of nifedipine. (C) Dose–response curve of Ni^{2+} reveals high potency in blocking I_{CaF} as compared with I_{CaS}, without an effect on the amplitude of I_{Na}. (D) Dose–response curve of nifedipine shows that the drug selectively suppresses I_{CaS} at a concentration range from 20 to 35 μM, with no effect on I_{Na}.

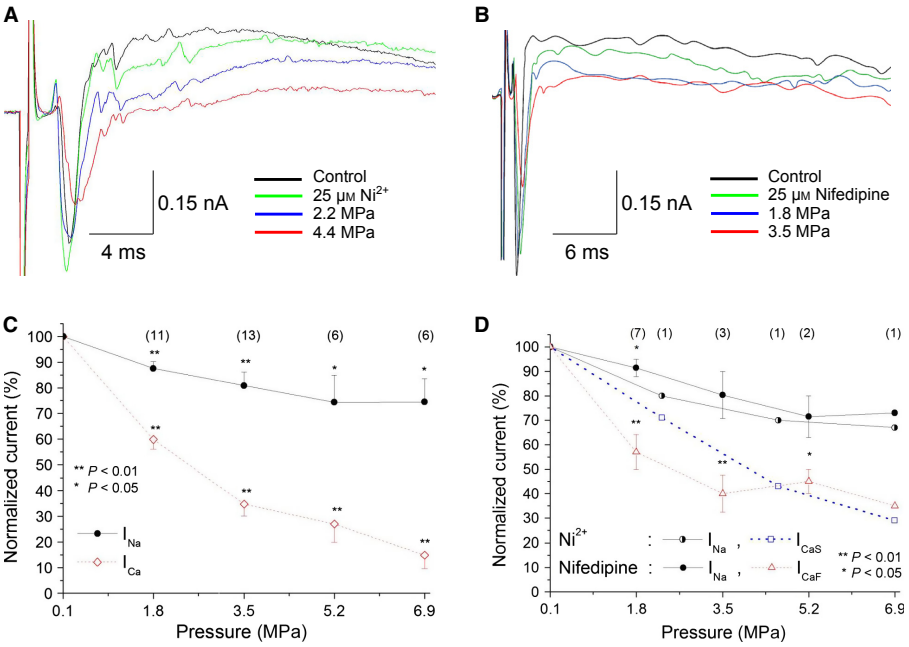

FIG. 5. High pressure (HP) depresses Ca^{2+} currents. Bars indicate standard errors of the mean; numbers in parentheses indicate *n*. (A) Traces recorded in the presence of Ni^{2+} with increasing pressure. (B) Traces recorded in the presence of nifedipine with increasing pressure. (C) HP depresses (85 ± 5% at 6.9 MPa) the maximal Ca^{2+} current amplitude of the early phase (I_{CaF}) in a dose-dependent manner, with a concomitant decrease in I_{Na} by 25 ± 9% at 6.9 MPa. Note a significant reduction in the Ca^{2+} current at a moderate pressure of 1.8 MPa. No Ca^{2+} blockers were used in this series of experiments. (D) HP effects on isolated I_{CaS} and I_{CaF}. Pressure depresses I_{CaS} (isolated by 25 μM Ni^{2+}) and I_{CaF} (isolated by 25 μM nifedipine) in a dose-dependent manner. Note, however, the relatively large reduction at the moderate pressure of 1.8 MPa. The effect on the Na^{+} current is similar to that in C.

Interaction of pressure and $[Ca^{2+}]_o$

The general effect of pressure on Ca^{2+} currents (Fig. 5) was examined at normal 1.8 mM $[Ca^{2+}]_o$. In order to estimate the $[Ca^{2+}]_o$–pressure interaction, the preparation was initially perfused with normal physiological solution during compression to 3.5 MPa (Fig. 6A, red trace). The expected depression of Ca^{2+} currents was observed. Then, the solution was changed to one containing 9 mM $[Ca^{2+}]_o$ (five-fold

© 2013 Federation of European Neuroscience Societies and John Wiley & Sons Ltd

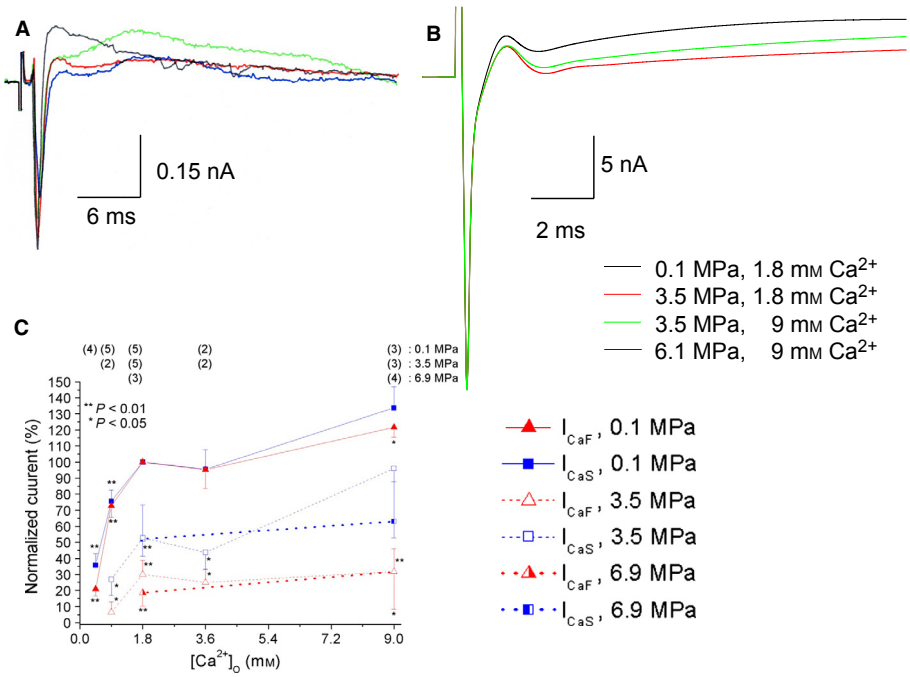

FIG. 6. (A) Pressure and $[Ca^{2+}]_o$ effects on the nerve terminal currents. All current records are from the same site, with the conditions specified in the legend. At normal 1.8 mM $[Ca^{2+}]_o$, pressure of 1.8 MPa (not shown) and 3.5 MPa (red trace) depresses the amplitudes of the fast and slow components of the Ca^{2+} current. Increasing $[Ca^{2+}]_o$ to 9 mM at a pressure of 3.5 MPa partially overcomes HP effects, especially on the slow component. Increasing the pressure to 6.1 MPa further depresses the Ca^{2+} currents, regardless of the elevated $[Ca^{2+}]_o$. (B) Computer simulation of HP and $[Ca^{2+}]_o$ effects on Ca^{2+} currents measured at the node remotely from the axon's terminal. (C) $[Ca^{2+}]_o$ effects on Ca^{2+} currents at pressure, as measured from A. At normal pressure (0.1 MPa), the normalised I_{CaF} (measured at 1–2 ms after the peak Na^+ current) and I_{CaS} (measured with a 10-ms delay) are similar in their response to increased $[Ca^{2+}]_o$. However, at 3.5 and 6.9 MPa, I_{CaF} saturates at a much lower level than I_{CaS}. Bars indicate standard errors of the mean; numbers in parentheses indicate *n*.

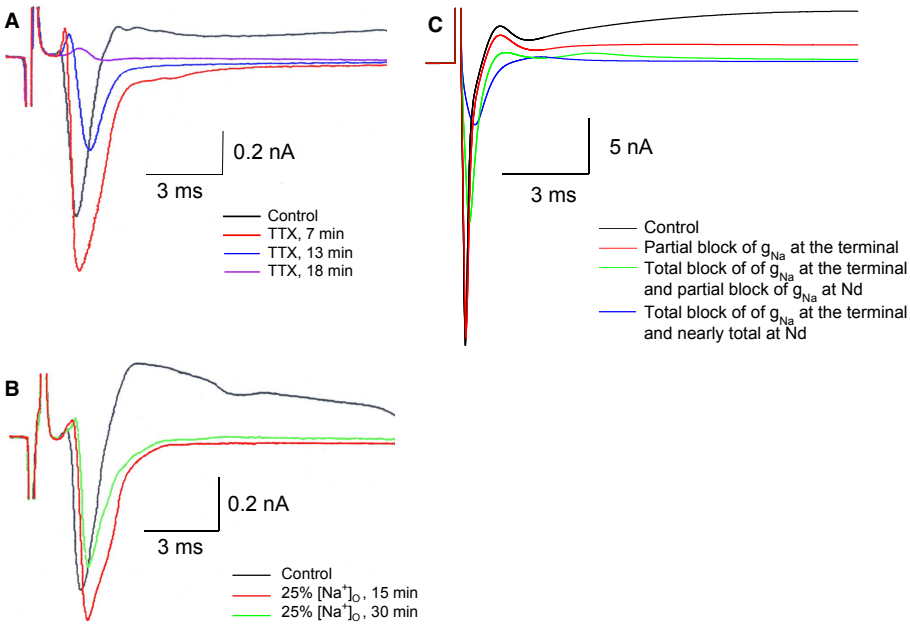

FIG. 7. Terminal currents under reduced Na^+ current conditions. (A) Nerve treated with 0.3 μM TTX. The duration of exposure is indicated. (B) Another nerve perfused with a solution in which 75% of the Na^+ was substituted with equimolar choline. The duration of exposure is indicated. Both treatments block the terminal Ca^{2+} current, whereas the Na^+ action current at the recording site is increased initially (see Discussion). Only with longer exposure is the Na^+ current diminished and ultimately blocked by TTX. (C) Computer simulation of progressive decrease of Na^+ conductance. Nd.

higher than the normal concentration). As a result, I_{CaS} was greatly increased (Fig. 6A, green trace), showing a recovery to a level even greater than that under control conditions (Fig. 6A, black trace). In contrast, I_{CaF} was not affected by the $[Ca^{2+}]_o$ increase, and remained ~70% depressed (Fig. 6A, green trace). Increasing the pressure to 6.1 MPa further suppressed the enhanced I_{CaS} to approximately its level at 3.5 MPa with normal $[Ca^{2+}]_o$ (Fig. 6A, blue trace). This result indicated different behavior of the two currents at various

© 2013 Federation of European Neuroscience Societies and John Wiley & Sons Ltd

TABLE 3. Channel blockade in simulation of pressure and $[Ca^{2+}]_o$ effects; the negative number indicates percentage increase

	Terminal (% block)				Node (% block)	
Step	g_{KDR}	g_{Ks}	g_{CaL}	g_{CaN}	g_{KDR}	Fig. 6(B)
a	100	100	40	80	80	Red line
b	100	100	–8	64	80	Green line

$[Ca^{2+}]_o$ levels. Therefore, an additional set of experiments was performed in which each preparation was exposed to various $[Ca^{2+}]_o$ levels at normal pressure and HP (Fig. 6C). It can clearly be seen that, at atmospheric pressure, the curves depicting a normalised current amplitude–$[Ca^{2+}]_o$ relationship were similar for both Ca^{2+} currents. However, at 3.5 MPa, the two curves, surprisingly, deviated from each other. I_{CaF} remained considerably more depressed than I_{CaS}, and could not be revamped by increasing $[Ca^{2+}]_o$. In contrast, increasing $[Ca^{2+}]_o$ to 9 mM boosted I_{CaS} almost up to the control level. Increasing $[Ca^{2+}]_o$ to 18 mM or even to 36 mM (n = 2) did not further enhance any of the currents (not shown).

High pressure of 6.9 MPa (Fig. 6C, dotted lines) similarly reduced the currents at 1.8 mM, but greatly reduced the ability of 9 mM $[Ca^{2+}]_o$ to boost I_{CaS}. This may indicate that there are fewer available channels to carry this current at pressure, as even five-fold $[Ca^{2+}]_o$ did not suffice to generate an increased flux through the remainder of less HP-affected channels. However, the two curves remained apart.

Simulation of pressure and $[Ca^{2+}]_o$ effects

In this set of experiments (Fig. 6C), 3.5 MPa decreased I_{CaF} by 70 ± 8% and I_{CaS} by 47 ± 11% at normal $[Ca^{2+}]_o$ of 1.8 mM (n = 5). In the model, I_{CaF} and I_{CaS} were simulated by N-type and L-type VDCCs, respectively (Fig. 6B, black line). Pressure effects were simulated (Table 3) as a first approximation by similar reductions in the corresponding g_{CaN} and g_{CaL}, whereas g_{Ks} were blocked at the terminal and at the node, imitating the TEA application (Fig. 6B, red line). In order to simulate the partial recovery of I_{Ca} when $[Ca^{2+}]_o$ was increased to 9 mM at 3.5 MPa (Fig. 6A and B, green trace), both g_{CaN} and g_{CaL} were increased by a factor of 1.8 (while g_{Ks} remained unchanged). The simulated enhancement of I_{Ca} under pressure and elevated $[Ca^{2+}]_o$ conditions appears to occur mainly at the I_{CaS} phase.

An attempt to evoke Ca^{2+} currents by reduced APs

In the experiments described so far, Ca^{2+} currents were induced by remotely evoked APs. As the Na^+ current component was also reduced by pressure (as previously reported for invertebrates; see Introduction) it was not clear whether pressure directly affects the VDCCs and/or has an indirect effect by reducing the amplitude of the AP invading the motor nerve terminal. A simple approach to answer this question could have been to correlate the Ca^{2+} currents under normal conditions with the amplitude of the pre-terminal Na^+ action current (recorded at the electrode site) reduced to levels observed with HP (Fig. 5C) by treatments other than pressure. This would have shown whether the HP-induced depression of Na^+ can solely explain the reduction in Ca^{2+} currents. In order to attenuate the AP amplitude, the preparations were perfused with either 0.1–1 μM tetrodotoxin (TTX) (n = 7) or 0–50% Na^+ solutions substituted with equimolar amounts of choline (n = 3) or *N*-methylglucamine (n = 4). Unfortunately, TTX (Fig. 7A; 7 min) and low $[Na^+]_o$ (25%; Fig. 7B; 15 min) first abolished the terminal Ca^{2+} currents (indicated by the positive deflection following the nodal Na^+ current), and therefore temporarily increased the apparent Na^+ current at the recording site. Only later, with continuous perfusion, was the Na^+ current at the recorded nodes also reduced, with conduction ultimately being blocked with TTX (Fig. 7A; 18 min). Conduction could also be blocked experimentally by using a solution with $[Na^+]_o$ = 0, but that usually required a long perfusion time (not shown). Despite the inability to perform the desired experiment, this revealed that the exposed heminode and the terminal are always blocked before the nodes under the nerve sheath at the recording site, similar to the time dependency of the K^+ current blockade (Fig. 2). The simulation of Na^+ current blockade supports this notion. Furthermore, the absence of the Ca^{2+} currents normally seen after the nodal inward Na^+ current strongly indicates that the AP at the terminal is blocked, and consequently the terminal Ca^{2+} currents and back reflection nodal K^+ current are missing (Fig. 3B). These unexpected findings set the basis for the use of TTX in the direct stimulation protocol (see below).

Simulation of I_{Na} blockade

The interesting time-dependent spatial differential blocking of the AP by TTX was simulated by decreasing g_{Na} in several steps (Fig. 7C; Table 4) as compared with a control of nodal current (black line) under similar conditions to those of Fig. 3C (black line).

The simulation verified the 'paradoxical' experimental observation, that I_{Ca} measured at the node can be reduced by TTX, even when the AP current at the node is not yet affected by the drug. This is a result of the reduction in the Na^+-dependent depolarising AP in the terminal that activates g_{Ca}. With additional time exposure (experimentally) and further reduction of g_{Na}, additional decrease of I_{Ca} concomitantly with a reduction in the nodal AP current were simulated. After blocking of g_{Na} at all segments, no currents could be recorded at the node (not shown).

Ca^{2+} currents induced by direct stimulation

As the attenuated AP approach could not be used to distinguish between the two mechanisms by which pressure might reduce the Ca^{2+} currents, the method of direct stimulation via the patch clamp amplifier was employed (see Materials and methods). In order to test the applicability of the new method, direct stimulation was compared with normal nerve stimulation in the same preparations (n = 5). Single direct stimulus with sufficient intensity elicited a Ca^{2+}-dependent response (Fig. 8E, 2) that was quite similar to that elicited by remote extracellular stimulation of the same nerve (Fig. 8E, 1). It is important to note that twin pulse interactions between the direct stimulus and the nerve stimulation indicated the existence of refractoriness between the two responses; that is, the direct stimulus elicited an AP that could

TABLE 4. Channel blockade in simulation of g_{Na} reduction

	Terminal (% block)		Node (% block)		
Step	g_{Na}	$g_{K(S\&DR)}$	g_{Na}	g_{KDR}	Fig. 7(C)
a	50	100	–	60	Red line
b	100	100	50	60	Green line
c	100	100	80	60	Blue line

© 2013 Federation of European Neuroscience Societies and John Wiley & Sons Ltd

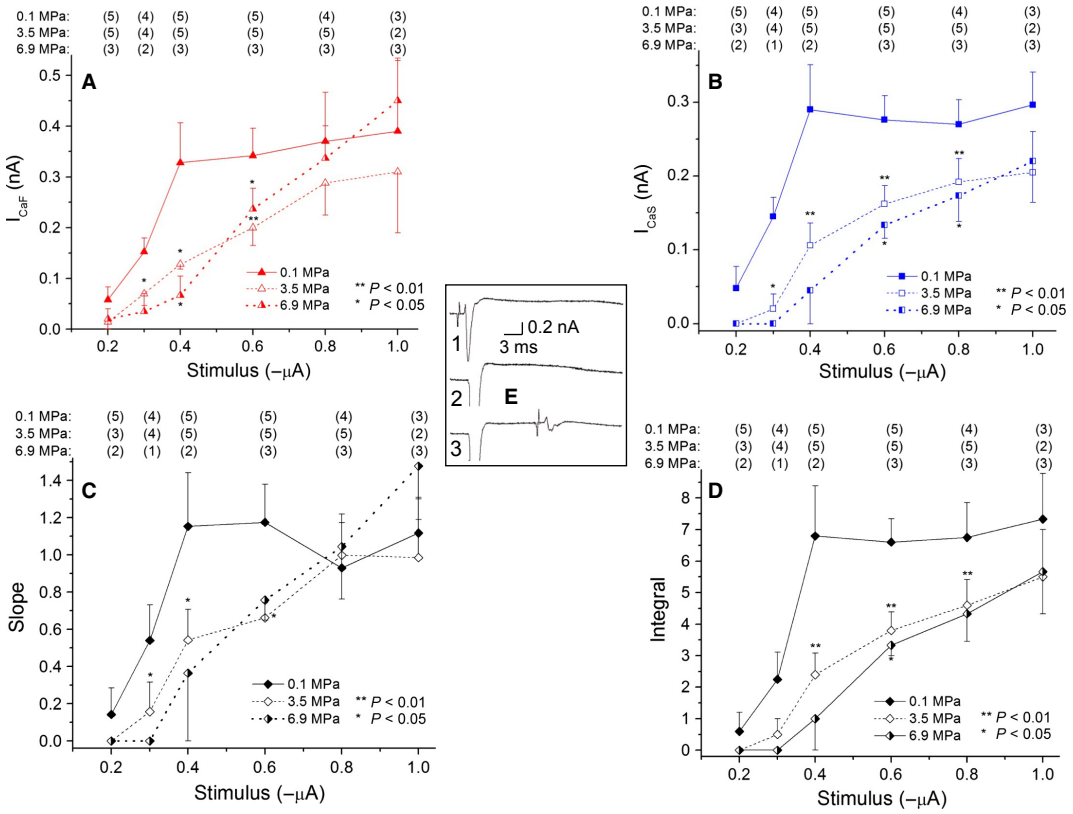

FIG. 8. Pressure effects on Ca^{2+} currents evoked by direct stimulation. Bars indicate standard errors of the mean; numbers in parentheses indicate *n*. (A) HP effects on the fast component of the Ca^{2+} current as a function of direct stimulus intensity (1 ms). (B) As in A for the slow component. (C) Initial slope of Ca^{2+} current. (D) Time integral of Ca^{2+} current. (E) Directly evoked (−0.5 μA, 1 ms) Ca^{2+} currents at normal pressure (2) are similar to those evoked by control nerve stimulation (1). Nerve stimulation in the same preparation demonstrates refractoriness after the direct stimulus (3).

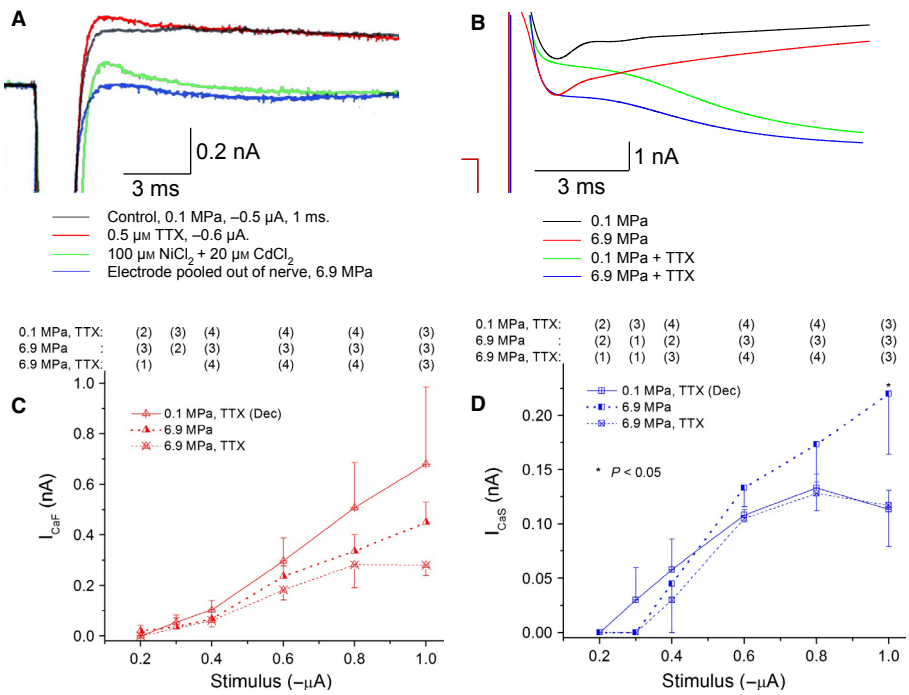

FIG. 9. Pressure effects on Ca^{2+} currents evoked by direct stimulation in TTX-treated nerves. (A) Experimental measurements. Black – control. Red – conduction is blocked. Green – blockade of Ca^{2+} currents. Blue – the electrode was pulled out of the nerve at HP, showing stability of the artefact compensation procedure (see Materials and methods). (B) Computer simulation of HP effects on naive and TTX-treated axons, directly stimulated at the node (see text for details). (C) HP effects on the fast component of the Ca^{2+} current as a function of direct stimulus intensity (1 ms). TTX (1 μM) was added at pressure (6.9 MPa). Values for normal pressure (0.1 MPa) were obtained after decompression (Dec, TTX is present). (D) As in C, for the slow component.

© 2013 Federation of European Neuroscience Societies and John Wiley & Sons Ltd

not be detected during the stimulus period (Fig. 8E, 3) (see below).

Ca^{2+} current amplitude

I_{CaF} and I_{CaS} were measured as the maximal amplitude at 0.5–2 and 12–15 ms after the stimulus artefact, respectively. A detailed description of the relationship between stimulus intensity and the averaged current responses of I_{CaF} (Fig. 8A) and I_{CaS} (Fig. 8B) is shown. Under normal conditions (0.1 MPa), the current threshold for a detectable Ca^{2+} response was 0.2 μA among different preparations. At stimulus intensities of 0.4–1.0 μA, both currents tended to saturate. Exposure to HP of 3.5 MPa shifted the curves to the right by 0.1–0.2 μA, and apparent saturation occurred at a stimulus range of 0.8–1.0 μA. The apparent saturation (measured at 1.0 μA) of I_{CaF} was reduced by 21%, and that of I_{CaS} was reduced by 31%. The reduction in the responses at 0.4 μA was much greater (by 61 and 63%, respectively). Further pressurising to 6.9 MPa reduced the mean currents at a stimulus intensity of 0.4 μA by 80% for I_{CaF} and by 84% for I_{CaS}. However, increased stimulus intensity could partially compensate for the reduction in I_{CaS} caused by the pressure increase, and more effectively for I_{CaF}. Nevertheless, the responses increased monotonically without showing any saturation level. This, in contrast to the control curves, may suggest that HP also reduces the contribution of the AP to the generation of the Ca^{2+} currents (see Discussion).

Ca^{2+} current initial slope

A simple estimate of pressure effects on the kinetics of the Ca^{2+} current could be derived by examining the change in the initial slope of the current, measured between 10 and 90% of the first peak. Obviously, this reflects mostly the behavior of I_{CaF}, which peaks between 0.5 and 2 ms after the end of the stimulus. Pressure of 3.5 MPa and additionally 6.9 MPa reduced the initial slope of the current at a stimulus range of 0.2–0.6 μA (Fig. 8C), where a curve shift of ~ 0.1 μA was observed for each pressure step. Stimulus intensities above 0.6 μA tended to compensate for the pressure effects, even at 6.9 MPa. Again, the response was saturating at stimulus intensities in the range of 0.6–1.0 μA at levels close to control values (note that the points at 1.0 μA are not statistically different). This is similar to the above mentioned observation of the amplitude change of I_{CaF}. The rightward shift in the curve, possibly resulting from reduced voltage sensitivity, and the compensation of the initial slope suggest that the slope is also controlled by the AP amplitude and its terminal distribution, rather than solely by pressure effects on the channel kinetics.

Ca^{2+} current time integral

As synaptic release is dependent on, among other factors, the amount of Ca^{2+} entry into the nerve terminal, it was of interest to examine pressure effects on the total ionic charge movement, estimated by the time integral of the current (measuring the area between the trace and baseline) during the first 30 ms (after which the recorded current has subsided). As the directly evoked Ca^{2+} current is relatively very long, the integral obviously reflects mainly I_{CaS}. Pressure of 3.5 MPa and additionally 6.9 MPa greatly reduced the time integral at 0.4 μA (65 and 85%, respectively) (Fig. 8D). The responses at pressure did not saturate at stimulus intensities in the range of 0.4–1.0 μA, but maximal stimulus intensity was able to partially compensate for the pressure induced depression, reaching up to 77% of control. HP shifted the curves to the right by ~0.1 μA for each pressure step. This shift, which is similar to the HP effect on the I_{CaS} amplitude (Fig. 8B), and the absence of full recovery strongly indicate that the integral reflects mostly the change in the amplitude of I_{CaS}.

Ca^{2+} current amplitude in the presence of TTX

The observed refractoriness, its similarity to nerve stimulation and the tendency for saturation of the Ca^{2+} currents at moderate stimulus intensities indicated that the direct stimulus (0.4 μA and above) evoked an AP in the axon (and its terminals), the current of which could not be detected because it coincides with the direct pulse stimulation that saturated the amplifier. Despite the above suggestion that high saturating stimulus intensities may reveal the channels' maximal response to pressure alone, repeating some of these experiments in the presence of TTX in order to eliminate the AP-dependent processes could be helpful. Therefore, the following experiments were carried out.

Initially, control Ca^{2+} currents evoked by direct stimulation were recorded (Fig. 9A, black trace). Then, TTX was added to the external solution under normal pressure conditions, and maintained throughout the experiment ($n = 2$). When conduction was completely blocked (similar to the experiment shown in Fig. 7A, 18 min), a similar Ca^{2+} current could be elicited with a slightly stronger current (Fig. 9A, red trace). This current was also Ca^{2+}-dependent, as perfusion with a solution containing both 20 μM Cd^{2+} and 100 μM Ni^{2+} (similar to Figs 3 and 5 for nerve stimulation) eliminated I_{CaS} and most of I_{CaF} (Fig. 9A, green trace). The remaining fast phase totally disappeared (while the stimulus artefact remained well compensated) when the electrode was pulled out of the nerve, even at high pressure (Fig. 9A, blue trace), thus providing assurance of the stability of the artefact compensation procedure. However, in order to monitor the stability of the recording during compression to 6.9 MPa (by frequently testing the response to the nerve stimulation), TTX was added in a different protocol after this critical compression step. Values for normal pressure were obtained after decompression was performed ($n = 3$). With this protocol, it was possible to compare pressure effects on naive vs. TTX-treated axons in the same preparation. Details of the pressure effects on the curves describing the relationship between the stimulus intensity and the Ca^{2+} currents are shown in Fig. 9C and D. The introduction of TTX into the solution at 6.9 MPa reduced both Ca^{2+} currents in response to a stimulus of ≥ 0.6 μA. The Ca^{2+} current increased monotonically with moderate stimulus intensities. In the presence of TTX, HP reduced I_{CaF} by 59% for the 1.0-μA stimulus intensity as compared with Ca^{2+} currents after decompression, whereas I_{CaS} was not affected. It seems again that I_{CaS} is less sensitive to HP than I_{CaF}, but the lack of any HP effect is in apparent contrast to the results for currents evoked by APs (see Discussion).

Simulation of pressure effects with local direct stimulation

The experimental results of the direct local stimulation (Fig. 8) and AP blockade by TTX (Fig. 9A, C, and D) suggest that the apparent reduction in I_{Ca} could result from a combination of pressure effects on both VDCCs and the AP.

In order to further clarify this point, we simulated I_{Ca} under the following specific conditions: (i) HP; (ii) normobaric pressure with g_{Na} blockade by TTX; and (iii) HP with TTX (Fig. 9B; Table 5). However, in preliminary simulations of direct stimulation, we encountered unstable responses (such as oscillations). Therefore, we

© 2013 Federation of European Neuroscience Societies and John Wiley & Sons Ltd

TABLE 5. Channel blockade in simulation of pressure effects using local direct stimulation

	Terminal (% block)				Node (% block)			
Step	$g_{Ca(F\&S)}$	g_K	g_{KDR}	g_{Na}	g_{KDR}	g_{Ks}	g_{Na}	Fig. 9(B)
a	33	100	100	–	50	–	–	Red line
b	–	100	100	100	90	57	100	Green line
c	33	100	100	100	97	67	100	Blue line

TABLE 6. The effects of Ca^{2+} channel blockers on preterminal Ca^{2+} currents

Ca^{2+} blocker	I_{CaF}	I_{CaS}	N
$CdCl_2$	10 (R)	10 (R)	4
$NiCl_2$	20–25	30–50 (R)	6
Nifedipine	40	20–25	7
Bay K 8644	NE (10)	6–8	3
w-Conotoxin	1–2 (P)	1–2 (P)	3
Phenytoin	50 (P)	50 (P)	3

NE, no effect; P, persistent; R, reversible. Concentrations in μM for ED_{50}. Numbers in parentheses indicate the maximal concentration used.

had to adjust the following control conductances (Fig. 9B, black line, in S/cm^2): at the terminal, $g_{Na} = 0.16$; at the node, $g_{KDR} = 0.32$, and $g_{Ks} = 0.7$.

Obviously, the stimulus currents are not compensated for by the simulation, and thus there is some distortion of the current lines in the first millisecond. However, the simulations suggest that, during direct stimulation, activation of AP-like response (which cannot be detected during the stimulus) contributes to the generation of I_{Ca}, because, under both normobaric and HP conditions, I_{Ca} is reduced in the absence of I_{Na}. Furthermore, even during the blockade of I_{Na}, the HP depression of I_{Ca} is still prominent, further supporting a direct HP effect on VDCCs.

Discussion

This study is the first direct analysis of presynaptic nerve terminal Ca^{2+} currents under HP conditions. Presynaptic Ca^{2+}-dependent mechanisms have already been implicated in pressure depression of evoked synaptic transmission (Grossman & Kendig, 1990; Grossman *et al.*, 1991a,b; Golan & Grossman, 1992). However, the present study clearly demonstrates that reduction in Ca^{2+} currents, i.e. Ca^{2+} entry into the nerve terminal, could be a major (although not the sole) cause for pressure depression of synaptic release. The differential pressure effects further support the notion that the motor nerve terminal entails at least two kinds of Ca^{2+} current (Lemos & Nowycky, 1989; Takahashi & Momiyama, 1993; Regehr & Mintz, 1994; Meir *et al.*, 1999; Fisher & Bourque, 2001; Reid *et al.*, 2003; Ishikawa *et al.*, 2005), I_{CaF} and I_{CaS}, which, in the frog, are likely to reflect N-like and L-like types of VDCC, respectively. These currents may play different physiological roles in synaptic release and respond variably to HP exposure (Talpalar *et al.*, 2010).

Methodology – recording conditions

The quality of the loose patch clamp recording was previously evaluated (Lindgren & Moore, 1991) by modeling such a recording at an exposed nerve terminal. It was concluded that the recording is quite localised; that is, the recorded currents originate at the membrane underneath the tip of the electrode, but may be sensitive to the distance (in μm) of the electrode from the membrane. The efficacy of the constant current stimulus was evaluated by Dudel (1981), who showed, surprisingly, very similar ranges of stimulus intensity for crayfish and frog (Parnas *et al.*, 1982) nerve terminals. We conclude that the loose patch clamp technique combined with recording under the perineurial sheath, where the voltage is clamped to ground potential in a confined space beneath the electrode tip, which increases the seal resistance (2–5 MΩ), has yielded a steady, reliable current measurement.

Another important question was how faithfully this type of recording in the nodal region (Fig. 1) reflects the currents flowing in the terminal zone. Mallart (1984, 1985) has already concluded that the nerve sheath allows K^+ and Ca^{2+} currents originating at the terminal to be recorded in the nodes, concomitantly with local Na^+ and K^+ currents (Dubois, 1981). However, the amplitude of the retrograde currents will be dependent on the distance (mm) from the terminal, as shown by Penner & Dreyer (1986) in mouse motor nerve terminals. Yet, relatively large currents can be measured at distances > 1 mm from the terminal [Fig. 2 of Penner & Dreyer (1986)]. The amplitude of the K^+ current in the present experiments was in the range of 30–50% of the Na^+ current, and the estimated distance from the terminals (based on visual inspection) was in the range of 0.3–1.0 mm. Furthermore, the extracellular current recorded from the exposed frog terminal at a location close to the terminal (myelin ending) is very similar to that found with our perineurial sheath loose patch clamp recording [Fig. 1A of Mallart (1984)].

Several additional observations support the assumption that the recording electrode (under the sheath) is electrically close enough to detect terminal currents: (i) when the AP was blocked at the terminals by TTX, the 'back reflection' current (as seen in Fig. 3B, blue trace) disappeared (Fig. 7A, red trace); (ii) the direct stimulation method in the presence of TTX could evoke voltage-dependent Ca^{2+} currents at the terminals – thus, the electrode was close enough to the terminal to support passive spread of the stimulus when AP propagation was blocked; (iii) similar direct stimulus parameters (duration and intensities) were utilised to evoke synaptic currents in exposed naive or TTX-treated terminals of similar frog preparations (Parnas *et al.*, 1982); and (iv) our theoretical simulations based on realistic morphological and ionic conductances have confirmed the interpretation of various experimental current phases. We conclude that the recordings faithfully reflect both the remote terminal and the local nodal currents.

Methodology – blocking I_K

As the present recording technique shows only the net summated current, there is always a possibility of specific currents masking each other. TEA (10 mM) was used to block all I_Ks in this preparation, in order to reveal I_{Ca}. A similar method was used successfully in frog (Mallart, 1984; Hevron *et al.*, 1986; Anderson *et al.*, 1988), mouse (Mallart, 1985; Penner & Dreyer, 1986) and lizard (Lindgren & Moore, 1989, 1991) terminals. Quite often, this procedure slightly diminished the Na^+ component of the current, owing to the canceling effect of the opposite polarity of I_{Ca} (Figs 2A and 3B). The possibility that, at a non-treated terminal, the remaining I_Ks are also reduced by HP, and thus enhance apparent I_{Ca} ('counteracting pressure effects'), could not be examined experimentally under TEA blockade. However, previous studies in voltage-clamped squid (Conti *et al.*, 1982) and lobster (Grossman & Kendig, 1984) axons revealed that pressure primarily increases the steady state I_K, suggesting that the HP effect on I_K in our study does not affect the

© 2013 Federation of European Neuroscience Societies and John Wiley & Sons Ltd

apparent I_{Ca}. Furthermore, we used the simulation model to more carefully examine the kinetics of I_K blockade. We were able to simulate the experimental time-dependent results (Fig. 2A) by first blocking only the terminal I_Ks without any influence on the nodal I_Ks. The latter response was simulated by totally blocking terminal I_K while the nodal I_Ks were only partly blocked (Fig. 2B, blue line). In most of the other simulations (e.g. TTX and compression), we had to leave a residual I_K in order to simulate the results, or, in rare extreme cases, to prevent membrane potential oscillations resulting from unbalanced I_{Ca}. Thus, it seems that TEA application did not totally eliminate I_K in the nodes.

In conclusion, it is conceivable that the amplitude of the measured I_{Ca} cannot be taken as the absolute value of that current. However, all of the methods, aided by the model simulations, are useful for measuring the relationships between the various components of the terminal currents and the relative changes caused to them by HP exposure.

Terminal Ca^{2+} currents at normal and high pressure

The close similarity between our results describing I_{Ca} as a function of the direct stimulus intensity (Figs 8B and C, and 9C and D), and the previously reported curve depicting the actual synaptic release in similar frog synapses as a function of the same stimulus currents (in both naive and TTX-treated terminals) (Parnas *et al.*, 1982), strongly indicates that our measured I_{Ca} is indeed associated with synaptic release. Our pharmacological tests, HP modulation and $[Ca^{2+}]_o$ changes in the frog nerve terminals revealed that this presynaptic I_{Ca} is composed of I_{CaF} [mediated by N-type VDCCs; see also Gundersen *et al.* (1982) and Katz *et al.* (1995)] and I_{CaS} (mediated by L-type VDCCs), which are common to many nerve terminals (Penner & Dreyer, 1986; Anderson & Harvey, 1987; Sher *et al.*, 1991; Fisher & Bourque, 2001; Reid *et al.*, 2003; Ishikawa *et al.*, 2005). The differential pressure sensitivity of I_{CaF} and the known pressure depression of synaptic transmission (see Introduction) seem to support the notion that the N-type VDCCs are mainly associated with the evoked release in the frog neuromuscular junction, whereas other types of channel may be more resistance to pressure (Etzion & Grossman, 2000). The slow L-type current, which is only moderately depressed by pressure, may also be involved in maintaining $[Ca^{2+}]_i$, as pressure also reduces the frequency of spontaneous miniature postsynaptic potentials in a similar preparation (Ashford *et al.*, 1982). Pressure also shifted the curve showing the relationship between I_{Ca} and direct stimulus current to the right. This change may indicate a comparable shift in the relationship between I_{Ca} and the actual membrane potential. A similar shift has been reported for I_{Na} of lobster axons under voltage clamp conditions (Grossman & Kendig, 1984).

Pressure selectively altered the relationship between I_{Ca} and $[Ca^{2+}]_o$. At normobaric pressure, the normalised curves for I_{CaS} and I_{CaF} were almost identical (Fig. 6C). At HP, both currents showed a tendency for saturation at levels below control, as predicted by Grossman & Kendig (1990), but the fast component was more depressed. This could also be attributed to a reduced number of functional Ca^{2+} channels that cannot be fully compensated for by elevated $[Ca^{2+}]_o$. A similar phenomenon was reported for crayfish synapses, in which pressure also revealed an otherwise undetectable dependency of the synaptic delay on $[Ca^{2+}]_o$ (Golan & Grossman, 1992).

Pressure effects on the naive terminal could be simulated by reducing N-type and L-type VDCC conductance, and the partial recovery at elevated $[Ca^{2+}]_o$ was successfully simulated by a proportional increase. Recently, Talpalar *et al.* (2010), using experimental data and mathematical modeling of central nervous system (dentate gyrus) synaptic responses, suggested that such a recovery could take place by increased flow through the least depressed channels, in this case the L-type channels, rather than the strongly inhibited channels, i.e. the terminal N-type channels.

The direct stimulation of naive and TTX-treated nerves (Figs 8 and 9, respectively) and the simulations of the general changes in I_{Ca} under these conditions (Fig. 9B) strongly indicate that HP directly depressed the currents through Ca^{2+} channels. However, they also suggest that the natural AP plays an important role in inducing terminal inward I_{Ca}, and is thus a part of the mechanism of pressure effect. In naive nerves, HP reduced both currents. On the other hand, in the absence of the AP (I_{Na} blockade in the simulation), the relative pressure depression of I_{CaF} (evoked by direct stimulation; Fig. 9C) was only 31% (as compared with 45% at naive terminals), whereas I_{CaS} was not affected. It seems that the pressure effect on the terminal I_{CaF} results from combined depression of the AP and the channels themselves, whereas the I_{CaS} channels seem to be resistant to pressure; most of the pressure effect is indirectly mediated by the AP depression. Thus, it is of importance to examine how faithfully the nodal I_{Na} reflects the terminal I_{Na}. It is also worth noting that, when I_{Ca} at the terminal was reduced by $[Ca^{2+}]_o$ modification (Fig. 3A) or nearly blocked by short-duration exposure to TTX (Fig. 7A, 7 min), the apparent nodal I_{Na} was either elongated or increased, respectively. It was only a few minutes later that the TTX blocked AP conduction at the node. The initial change is probably attributable to summation of local and reflected currents (detailed in Ca^{2+} currents evoked by reduced APs). Thus, the presently reported small (10–15%) pressure depression of the nodal I_{Na} might be slightly underestimated. In fact, pressure diminution of the terminal I_{Na} of up to 30% was reported for crustacean neuromuscular synapses (Grossman *et al.*, 1991a; Golan & Grossman, 1992) and the presynaptic volley in mammalian brain slices (Etzion & Grossman, 2000; Talpalar & Grossman, 2003).

General considerations

The molecular basis for pressure effects is not clear. The differential effects of HP on various channels (Aviner *et al.*, 2009, 2010) or even a lack of effect (Heinemann *et al.*, 1987; Etzion & Grossman, 1999; Aviner *et al.*, 2011) are difficult to explain by a single mechanism. However, it is possible to speculate that, at moderate pressures, the primary target is the phospholipid membrane phase state, and the diversity of the response is the result of the specific interaction of each protein with the cell membrane. Other possible mechanisms could be related to minute structural differences between the various Ca^{2+} channels that lead to different conformational changes and variable activation volumes. HP may also affect some channel regulation pathways.

The complex effects of pressure on the two types of physiologically different presynaptic Ca^{2+} currents, i.e. reduction in amplitude, decrease in maximal (saturated) current, and possible shift in voltage dependency, in addition to concomitant diminution of the Na^+ AP, constitute the major basis of pressure depression of synaptic transmission that contributes, in part, to HP neurological syndrome (HPNS).

HP neurological syndrome is a term used to encompass a group of signs and symptoms arising in the majority of living organisms when they are exposed to HP. The level of pressure sufficient to trigger this phenomenon seems to be species-dependent: complete

© 2013 Federation of European Neuroscience Societies and John Wiley & Sons Ltd

seizures have been seen in fish at 5–13 MPa, in reptiles at 10–13 MPa, in birds at 10–12 MPa, in mammals at 7–9 MPa, and in primates at 6–10 MPa (Macdonald, 1982). Over 22 species of vertebrate have been exposed to pressure, and all have shown the same basic pattern of motor effects.

HP neurological syndrome affects professional deep sea divers, who are routinely exposed to pressure > 1 MPa, with both motor and cognitive manifestations (Logue *et al.*, 1986; Vaernes *et al.*, 1988; Abraini, 1997), including visual and auditory deficiencies, impaired coordination, sleep disorders, dizziness, and nausea. These alone may impact on the divers' performance and safety under water, but even more dangerous seizures, convulsions and loss of consciousness may also evolve, posing a serious threat to their lives when they are working at extreme depths. HPNS generally manifests as nervous hyperexcitability, but most findings to date have suggested a depression of synaptic mechanisms at pressure. The observed selective pressure effect on different types of VDCC (even within the same family) may provide a rationale through which this contradiction can be explained.

Further direct current measurements in VDCCs are needed in order to elucidate the HPNS mechanism.

Acknowledgements

This work was supported by USA ONR grants no. N00014-91-J-1908 (early phase) and no. N00014-10-1-0163 (recent phase) to Y. Grossman. We thank Drs Y. Yaari and E. Hevron, who introduced Y. Grossman to the preparation, Mrs K. Miller for skilfull technical support, and Ms S. Aviner for her dedicated graphical assistance.

Abbreviations

AP, action potential; g_{Ca}, Ca^{2+}; g_{CaL}, L-type Ca^{2+}; g_{CaN}, N-type Ca^{2+}; g_{KDR}, delayed rectifier K^+; g_{Ks}, slow K^+ conductance density; g_{Na}, Na^+; HP, high pressure; HPNS, high-pressure neurological syndrome; I_{CaF}, fast Ca^{2+} current; I_{CaS}, slow Ca^{2+} current; I_K, K^+ current; I_{Na}, Na^+ current; TEA, tetraethyl ammonium; TTX, tetrodotoxin; VDCC, voltage-dependent Ca^{2+} channel.

References

Abraini, J.H. (1997) Inert gas and raised pressure: evidence that motor decrements are due to pressure per se and cognitive decrements due to narcotic action. *Pflug. Arch.*, **433**, 788–791.

Anderson, A.J. & Harvey, A.L. (1987) Omega-conotoxin does not block the verapamil-sensitive calcium channels at mouse motor nerve terminals. *Neurosci. Lett.*, **82**, 177–180.

Anderson, A.J., Harvey, A.L., Rowan, E.G. & Strong, P.N. (1988) Effects of charybdotoxin, a blocker of Ca^{2+}-activated K^+ channels, on motor nerve terminals. *Brit. J. Pharmacol.*, **95**, 1329–1335.

Artim, D.E. & Meriney, S.D. (2000) G-protein-modulated Ca(2+) current with slowed activation does not alter the kinetics of action potential-evoked Ca(2+) current. *J. Neurophysiol.*, **84**, 2417–2425.

Ashford, M.L., MacDonald, A.G. & Wann, K.T. (1982) The effects of hydrostatic pressure on the spontaneous release of transmitter at the frog neuromuscular junction. *J. Physiol.*, **333**, 531–543.

Aviner, B., Gnatek, Y., Gradwohl, G. & Grossman, Y. (2010) Hyperbaric pressure effects on voltage-dependent Ca^{2+} channels: relevance to HPNS. *Undersea Hyperbar. M.*, **37**, 245–258.

Aviner, B., Mor, M. & Grossman, Y. (2009) Pressure modulation of Ca^{2+} channel activity may elucidate HPNS mechanisms. In: Proceedings European Undersea Baromedical Society, 35th Annual Meeting, Aberdeen, Scotland.

Aviner, B., Mor, M. & Grossman, Y. (2011) P/Q type voltage dependent Ca^{2+} channel ($Ca_V2.1$) seems resistant to hyperbaric pressure. In: Proceedings Undersea and Hyperbaric Medical Society, 44th Annual Scientific Meeting, Fort Worth, TX, 83.

Bean, B.P. (1989) Classes of calcium channels in vertebrate cells. *Annu. Rev. Physiol.*, **51**, 367–384.

Boland, L.M. & Bean, B.P. (1993) Modulation of N-type calcium channels in bullfrog sympathetic neurons by luteinizing hormone-releasing hormone: kinetics and voltage dependence. *J. Neurosci.*, **13**, 516–533.

Booth, V., Rinzel, J. & Kiehn, O. (1997) Compartmental model of vertebrate motoneurons for Ca^{2+}-dependent spiking and plateau potentials under pharmacological treatment. *J. Neurophysiol.*, **78**, 3371–3385.

Braun, M. & Schmidt, R.F. (1966) Potential changes recorded from the frog motor nerve terminal during its activation. *Pflug. Arch. Ges. Phys.*, **287**, 56–80.

Brigant, J.L. & Mallart, A. (1982) Presynaptic currents in mouse motor endings. *J. Physiol.*, **333**, 619–636.

Byerly, L., Chase, P.B. & Stimers, J.R. (1984) Calcium current activation kinetics in neurones of the snail *Lymnaea stagnalis*. *J. Physiol.*, **348**, 187–207.

Campenot, R.B. (1975) The effects of high hydrostatic pressure on transmission at the crustacean neuromuscular junction. *Comp. Biochem. Phys. B*, **52**, 133–140.

Catterall, W.A. (2000) Structure and regulation of voltage-gated Ca^{2+} channels. *Annu. Rev. Cell Dev. Bi.*, **16**, 521–555.

Colton, C.A. & Colton, J.S. (1982) An electrophysiological analysis of oxygen and pressure on synaptic transmission. *Brain Res.*, **251**, 221–227.

Conti, F., Fioravanti, R., Segal, J.R. & Stuhmer, W. (1982) Pressure dependence of the potassium currents of squid giant axon. *J. Membrane Biol.*, **69**, 35–40.

Dubois, J.M. (1981) Evidence for the existence of three types of potassium channels in the frog Ranvier node membrane. *J. Physiol.*, **318**, 297–316.

Dudel, J. (1981) The effect of reduced calcium on quantal unit current and release at the crayfish neuromuscular junction. *Pflug. Arch.*, **391**, 35–40.

Etzion, Y. & Grossman, Y. (1999) Spontaneous Na^+ and Ca^{2+} spike firing of cerebellar Purkinje neurons at high pressure. *Pflug. Arch.*, **437**, 276–284.

Etzion, Y. & Grossman, Y. (2000) Pressure-induced depression of synaptic transmission in the cerebellar parallel fibre synapse involves suppression of presynaptic N-type Ca^{2+} channels. *Eur. J. Neurosci.*, **12**, 4007–4016.

Fisher, T.E. & Bourque, C.W. (2001) The function of Ca(2+) channel subtypes in exocytotic secretion: new perspectives from synaptic and non-synaptic release. *Prog. Biophys. Mol. Bio.*, **77**, 269–303.

Formenti, A., Martina, M., Plebani, A. & Mancia, M. (1998) Multiple modulatory effects of dopamine on calcium channel kinetics in adult rat sensory neurons. *J. Physiol.*, **509**(Pt 2), 395–409.

Gilman, S.C., Colton, J.S. & Dutka, A.J. (1989) Pressure-dependent changes in the release of GABA by cerebrocortical synaptosomes. *Undersea Biomed. Res.*, **16**, 253–258.

Gilman, S.C., Colton, J.S., Dutka, A.J. & Boogaard, J.S. (1986a) Effects of high pressure on the release of excitatory amino acids by brain synaptosomes. *Undersea Biomed. Res.*, **13**, 397–406.

Gilman, S.C., Kumaroo, K.K. & Hallenbeck, J.M. (1986b) Effects of pressure on uptake and release of calcium by brain synaptosomes. *J. Appl. Physiol.*, **60**, 1446–1450.

Golan, H. & Grossman, Y. (1992) Synaptic transmission at high pressure: effects of [Ca2+]o. *Comp. Biochem. Physiol. Comp. Physiol.*, **103**, 113–118.

Grossman, Y. & Kendig, J.J. (1984) Pressure and temperature: time-dependent modulation of membrane properties in a bifurcating axon. *J. Neurophysiol.*, **52**, 693–708.

Grossman, Y. & Kendig, J.J. (1986) Pressure and temperature modulation of conduction in a bifurcating axon. *Undersea Biomed. Res.*, **13**, 45–61.

Grossman, Y. & Kendig, J.J. (1988) Synaptic integrative properties at hyperbaric pressure. *J. Neurophysiol.*, **60**, 1497–1512.

Grossman, Y. & Kendig, J.J. (1990) Evidence for reduced presynaptic Ca^{2+} entry in a lobster neuromuscular junction at high pressure. *J. Physiol.*, **420**, 355–364.

Grossman, Y., Colton, J.S. & Gilman, S.C. (1991a) Interaction of Ca-channel blockers and high pressure at the crustacean neuromuscular junction. *Neurosci. Lett.*, **125**, 53–56.

Grossman, Y., Colton, J.S. & Gilman, S.C. (1991b) Reduced Ca currents in frog nerve terminals at high pressure. *Ann. NY Acad. Sci.*, **635**, 411–412.

Grossman, Y., Parnas, I. & Spira, M.E. (1979) Differential conduction block in branches of a bifurcating axon. *J. Physiol.*, **295**, 283–305.

Gundersen, C.B., Katz, B. & Miledi, R. (1982) The antagonism between botulinum toxin and calcium in motor nerve terminals. *P. Roy. Soc. Lond. B Bio.*, **216**, 369–376.

Heinemann, S.H., Conti, F., Stuhmer, W. & Neher, E. (1987) Effects of hydrostatic pressure on membrane processes. Sodium channels, calcium channels, and exocytosis. *J. Gen. Physiol.*, **90**, 765–778.

© 2013 Federation of European Neuroscience Societies and John Wiley & Sons Ltd

Henderson, J.V., Lowenhaupt, M.T. & Gilbert, D.L. (1977) Helium pressure alteration of function in squid giant synapse. *Undersea Biomed. Res.*, **4**, 19–26.

Hess, P. (1990) Calcium channels in vertebrate cells. *Annu. Rev. Neurosci.*, **13**, 337–356.

Hevron, E., David, G., Arnon, A. & Yaari, Y. (1986) Acetylcholine modulates two types of presynaptic potassium channels in vertebrate motor nerve terminals. *Neurosci. Lett.*, **72**, 87–92.

Hines, M. (1989) A program for simulation of nerve equations with branching geometries. *Int. J. Biomed. Comput.*, **24**, 55–68.

Ishikawa, T., Kaneko, M., Shin, H.-S. & Takahashi, T. (2005) Presynaptic N-type and P/Q-type Ca^{2+} channels mediating synaptic transmission at the calyx of Held of mice. *J. Physiol.*, **568**, 199–209.

Katz, E., Ferro, P.A., Cherksey, B.D., Sugimori, M., Llinas, R. & Uchitel, O.D. (1995) Effects of Ca^{2+} channel blockers on transmitter release and presynaptic currents at the frog neuromuscular junction. *J. Physiol.*, **486**, 695–706.

Kendig, J.J. & Cohen, E.N. (1976) Neuromuscular function at hyperbaric pressures: pressure–anesthetic interactions. *Am. J. Physiol.*, **230**, 1244–1249.

Kendig, J.J., Trudell, J.R. & Cohen, E.N. (1975) Effects of pressure and anesthetics on conduction and synaptic transmission. *J. Pharmacol. Exp. Ther.*, **195**, 216–224.

Lemos, J.R. & Nowycky, M.C. (1989) Two types of calcium channels coexist in peptide-releasing vertebrate nerve terminals. *Neuron*, **2**, 1419–1426.

Lindgren, C.A. & Moore, J.W. (1989) Identification of ionic currents at presynaptic nerve endings of the lizard. *J. Physiol.*, **414**, 201–222.

Lindgren, C.A. & Moore, J.W. (1991) Calcium current in motor nerve endings of the lizard. *Ann. NY Acad. Sci.*, **635**, 58–69.

Logue, P.E., Schmitt, F.A., Rogers, H.E. & Strong, G.B. (1986) Cognitive and emotional changes during a simulated 686-m deep dive. *Undersea Biomed. Res.*, **13**, 225–235.

Macdonald, A.G. (1982) *Hydrostatic Pressure Physiology*. Balliere Tindall, London.

Macdonald, A.G., Ramsey, R.L., Drewry, J. & Usherwood, P.N. (1993) Effects of high pressure on the channel gated by the quisqualate-sensitive glutamate receptor of locust muscle and its blockade by ketamine; a single-channel analysis. *Biochim. Biophys. Acta*, **1151**, 13–20.

Mallart, A. (1984) Presynaptic currents in frog motor endings. *Pflug. Arch.*, **400**, 8–13.

Mallart, A. (1985) Electric current flow inside perineurial sheaths of mouse motor nerves. *J. Physiol.*, **368**, 565–575.

Meir, A., Ginsburg, S., Butkevich, A., Kachalsky, S.G., Kaiserman, I., Ahdut, R., Demirgoren, S. & Rahamimoff, R. (1999) Ion channels in presynaptic nerve terminals and control of transmitter release. *Physiol. Rev.*, **79**, 1019–1088.

Mor, A., Levy, S., Hollmann, M. & Grossman, Y. (2008) Differential effect of high pressure on NMDA receptor currents in *Xenopus laevis* oocytes. *Diving Hyperb. Med.*, **38**, 194–196.

O'Connell, K.M. & Dirksen, R.T. (2000) Prolonged depolarization promotes fast gating kinetics of L-type Ca^{2+} channels in mouse skeletal myotubes. *J. Physiol.*, **529**(Pt 3), 647–659.

Parmentier, J.L., Shrivastav, B.B. & Bennett, P.B. (1981) Hydrostatic pressure reduces synaptic efficiency by inhibiting transmitter release. *Undersea Biomed. Res.*, **8**, 175–183.

Parnas, I., Parnas, H. & Dudel, J. (1982) Neurotransmitter release and its facilitation in crayfish muscle. V. Basis for synapse differentiation of the fast and slow type in one axon. *Pflug. Arch.*, **395**, 261–270.

Penner, R. & Dreyer, F. (1986) Two different presynaptic calcium currents in mouse motor nerve terminals. *Pflug. Arch.*, **406**, 190–197.

Regehr, W.G. & Mintz, I.M. (1994) Participation of multiple calcium channel types in transmission at single climbing fiber to Purkinje cell synapses. *Neuron*, **12**, 605–613.

Reid, C.A., Bekkers, J.M. & Clements, J.D. (2003) Presynaptic Ca^{2+} channels: a functional patchwork. *Trends Neurosci.*, **26**, 683–687.

Shelton, C.J., Doyle, M.G., Price, D.J., Daniels, S. & Smith, E.B. (1993) The effect of high pressure on glycine- and kainate-sensitive receptor channels expressed in *Xenopus* oocytes. *P. Roy. Soc. B-Biol. Sci.*, **254**, 131–137.

Shelton, C.J., Zhao, D.M., Inman, N., Price, D.J., Daniels, S. & Smith, E.B. (1990) The effects of anesthetics and pressure on a synaptic receptor from the mamalian central nervous system expressed in *Xenopus* oocytes. In Drouet, J., Risso, J.J. & Rostain, J.C. (Eds), *Proceedings of the 2nd International Meeting on High Pressure Biology*. EASSM-CERB, Toulon, pp. 12.

Sher, E., Biancardi, E., Passafaro, M. & Clementi, F. (1991) Physiopathology of neuronal voltage-operated calcium channels. *FASEB J.*, **5**, 2677–2683.

Stanfield, P.R. (1983) Tetraethylammonium ions and the potassium permeability of excitable cells. *Rev. Physiol. Bioch. P.*, **97**, 1–67.

Stanley, E.F. (1989) Calcium currents in a vertebrate presynaptic nerve terminal: the chick ciliary ganglion calyx. *Brain Res.*, **505**, 341–345.

Takahashi, T. & Momiyama, A. (1993) Different types of calcium channels mediate central synaptic transmission. *Nature*, **366**, 156–158.

Talpalar, A.E. & Grossman, Y. (2003) Modulation of rat corticohippocampal synaptic activity by high pressure and extracellular calcium: single and frequency responses. *J. Neurophysiol.*, **90**, 2106–2114.

Talpalar, A.E., Giugliano, M. & Grossman, Y. (2010) Enduring medial perforant path short-term synaptic depression at high pressure. *Front. Cell Neurosci.*, **4**, 128.

Traub, R.D. & Miles, R. (1991) Multiple modes of neuronal population activity emerge after modifying specific synapses in a model of the CA3 region of the hippocampus. *Ann. NY Acad. Sci.*, **627**, 277–290.

Tsien, R.W., Lipscombe, D., Madison, D.V., Bley, K.R. & Fox, A.P. (1988) Multiple types of neuronal calcium channels and their selective modulation. *Trends Neurosci.*, **11**, 431–438.

Vaernes, R.J., Bergan, T. & Warncke, M. (1988) HPNS effects among 18 divers during compression to 360 msw on heliox. *Undersea Biomed. Res.*, **15**, 241–255.

Yaari, Y., Hamon, B. & Lux, H.D. (1987) Development of two types of calcium channels in cultured mammalian hippocampal neurons. *Science*, **235**, 680–682.

Yu, F.H. & Catterall, W.A. (2004) The VGL-chanome: a protein superfamily specialized for electrical signaling and ionic homeostasis. *Sci. STKE*, **2004**, re15.

© 2013 Federation of European Neuroscience Societies and John Wiley & Sons Ltd